Materials Research Bulletin 65 (2015) 116–122

Contents lists available at ScienceDirect

Materials Research Bulletin

journal homepage: www.elsevier.com/locate/matresbu

Crystal structure and oxygen storage properties of $BaLnMn_2O_{5+\delta}$ (Ln: Pr, Nd, Sm, Gd, Dy, Er and Y) oxides

Alicja Klimkowicz [a,b], Konrad Świerczek [a,*], Akito Takasaki [b], Janina Molenda [a], Bogdan Dabrowski [c]

[a] AGH University of Science and Technology, Faculty of Energy and Fuels, Department of Hydrogen Energy, al. A. Mickiewicza 30, 30-059 Krakow, Poland
[b] Shibaura Institute of Technology, Department of Engineering Science and Mechanics, 3-7-5 Toyosu, Koto-ku, 135-8548 Tokyo, Japan
[c] Northern Illinois University, Department of Physics, DeKalb, 60115 IL, USA

ARTICLE INFO

Article history:
Received 26 March 2014
Received in revised form 30 December 2014
Accepted 14 January 2015
Available online 15 January 2015

Keywords:
Oxides
Thermogravimetric analysis (TGA)
X-ray diffraction
Crystal structure
Energy storage

ABSTRACT

In this paper we report on crystal structure and oxygen storage properties of A-site cation ordered $BaLnMn_2O_{5+\delta}$ (Ln: Pr, Nd, Sm, Gd, Dy, Er and Y) perovskite-type oxides. The materials show practically complete and reversible change between fully reduced $BaLnMn_2O_5$ and oxidized $BaLnMn_2O_6$, which occurs at moderate temperatures (300–500 °C) during changes of the oxygen partial pressure (air, 5 vol.% H_2 in Ar). Based on the thermogravimetric measurements, reversible oxygen storage capacity, characteristic temperature of oxidation and reduction, as well as kinetics of these processes are given. Structural characterization was performed at room temperature for the reduced and oxidized materials by Rietveld analysis of the XRD data. These results are accompanied by *in situ* high temperature XRD measurements of the oxidation process, performed for $BaNdMn_2O_5$ in air.

1. Introduction

Recently, oxygen storage materials (OSMs) attracted scientific interest due to their possible usage in various processes, in which a precise control of the oxygen partial pressure (pO_2) is required [1–6]. Apart from commercial application in three-way catalysts, in which the best known CeO_2–ZrO_2 solid solution-type oxides are utilized [7], OSMs may be possibly used in many developing technologies and industrial processes, e.g.: in air separation technology, solar water splitting, non-aerobic oxidation including flameless combustion of hydrocarbons, high-temperature production that requires high-purity oxygen, oxy-fuel and chemical looping combustion processes used in clean coal-type energy production, production of synthesis gas, SOFC technology, inert gas purification due to oxygen scavenger behavior, etc. [1,8–11].

While ceria-based materials may be further modified [12,13], also new compounds were studied, including Pr_2O_2S–$Pr_2O_2SO_4$ system, which exhibit unusually high theoretical capacity of the order of 18.50 wt.% (practical one ~9.3 wt.% at 700 °C), but suffers from evaporation of sulfur [11]. Recently, also $BaLnMn_2O_{5+\delta}$ perovskite-type oxides gained scientific interest in terms of their applicability as oxygen storage materials [1,14–16]. As reported by Motohashi et al., the $BaYMn_2O_5$–$BaYMn_2O_6$ system with a theoretical capacity equal to 3.85 wt.% shows high reversibility and practical capacity ~3.7 wt.% at 500 °C. This system shows reduced temperatures of reduction and oxidation processes, and fast kinetics of changes of δ occurring at 500 °C [1].

From the crystallographic point of view, both, reduced $BaYMn_2O_5$ and oxidized $BaYMn_2O_6$ belong to a family of A-site cation ordered $BaLnMn_2O_{5+\delta}$ manganites with layer-type ordering, for which the structure can be derived from that of a simple perovskite. It is known that a significant difference between ionic radius and/or oxidation state of cations occupying at the same time A- or B-site in ABO_3 are the causes responsible for the cation ordering [17]. Commonly, 1:1-, 1:2- or 1:3-type structures are observed. The mentioned $BaLnMn_2O_5$ and $BaLnMn_2O_6$ are the examples of 1:1-type order, in which Ba–Ln ordering occurs in a form of layers [18–22].

In the case of A-site 1:1 layered order, the aristotype space group is tetragonal *P*4/*mmm* with doubling of the perovskite-related unit cell along *c*-axis [23]. In addition, depending on the Ln cation size, B-site rock salt-type cation ordering also occurs in $BaLnMn_2O_{5+\delta}$, giving rise to quite a complicated electronic structure diagram [20–22,24]. Oxygen anions, occupying positions within Ln-related layer can be extracted from the material relatively easy, and as was shown for $BaYMn_2O_{5+\delta}$, reduced

* Corresponding author. Tel.: +48 126174926.
E-mail address: xi@agh.edu.pl (K. Świerczek).

http://dx.doi.org/10.1016/j.materresbull.2015.01.041
0025-5408/

$BaYMn_2O_5$ and $BaYMn_2O_{5.5}$ compounds exist, with structure originating from removal of all (for O_5) and every other (for $O_{5.5}$) oxygen from the mentioned positions [4,16,25].

Structural and oxygen storage-related properties of $BaLnMn_2O_{5+\delta}$ are expected to be dependent on the ionic size of Ln^{3+} cations. In this work, we report results of crystal structure of $BaLnMn_2O_5$ and $BaLnMn_2O_6$, together with reduction/oxidation behavior of the considered oxides in different atmospheres. The results are analyzed in terms of the influence of ionic radii of Ln^{3+}, its electronegativity, as well as microstructure and specific surface area of the analyzed powders.

2. Experimental

$BaLnMn_2O_{5+\delta}$ (Ln: Pr, Nd, Sm, Gd, Dy, Er and Y) oxides with $\delta \approx 0$ were synthesized by a soft chemistry method. Respective nitrates were dissolved in small amount of deionized water, in stoichiometric proportions. Ammonia salt of ethylenediaminetetraacetic acid (EDTA) was added to the solutions, due to its complexing properties. Prepared mixtures were heated in quartz evaporators in air, up to about 400 °C. The heating process resulted in: an evaporation of water, a sol–gel transition, a decomposition of ammonium nitrite and finally, an oxidation of residual carbon, originating from EDTA. The obtained precursors were thoroughly ground and pressed into pellets having thickness of about 1 mm. The actual synthesis for $BaLnMn_2O_{5+\delta}$ (Ln: Pr, Nd, Sm, Gd and Y) was performed at 1100 °C, for 8 h in atmosphere of 1 vol.% of H_2 in Ar, with flow of gas of about 100 $cm^3\,min^{-1}$. In the case of $BaDyMn_2O_{5+\delta}$ sample, annealing was repeated three times, with intermediate grindings, and final temperature of 1000 °C. Synthesis method for $BaErMn_2O_{5+\delta}$ oxide, i.e., material with the smallest +3 cation being successfully introduced in Ln position, was described in the other paper [14]. For comparison, $BaNdMn_2O_{5+\delta}$ and $BaYMn_2O_{5+\delta}$ were also prepared by a standard solid state reaction. In this paper these samples are referred as, for example, $BaNdMn_2O_5$ II.

Structural studies of the synthesized oxides were carried out in 10–110° range with CuKα radiation, using Panalytical Empyrean diffractometer. Data were collected on as prepared materials, as well as after reduction and oxidation. For high-temperature measurements, Anton Paar HTK 1200N oven-chamber was installed. Measurements of the oxidation of reduced $BaNdMn_2O_5$, as well as studies for oxidized $BaNdMn_2O_6$ were performed in air. For Rietveld analysis, GSAS/EXPGUI set of software was used [26,27]. For clarity of presentation of the graphs, CuKα2 was stripped from the data by Rachinger method. The measurements were performed at 25 °C and in 100–800 °C range with 100 °C step, with heating rate of 10°C min^{-1}. Before 55 min collection of data, samples were equilibrated for 5 min at each temperature.

Oxygen storage-related properties, including reduction/oxidation runs, were determined by usage of thermogravimetric (TG) method. All experiments were conducted on TA Q5000IR apparatus. Measurements were done on powdered samples, obtained after grinding of sinters and sieving on 100 μm sieve. Atmosphere of 5 vol.% H_2 in Ar was used for the reduction, while the oxidation process was studied in synthetic air flow. For all studies, gas flow of 100 $cm^3\,min^{-1}$ and heating rate of 5°C min^{-1} were set up as the experimental conditions. Isothermal reduction/oxidation runs were collected at 500 °C, data shown in graphs concern 1st, 2nd or 5th cycle. Non-isothermal oxidations and reductions were collected after these five isothermal cycles. Calculation of the reversible oxygen storage capacity was corrected for buoyancy effect, which was established on a basis of runs performed without material (TG pan only).

Microstructural images of the reduced and oxidized materials were recorded on FEI Nova NanoSEM 200 microscope equipped with low vacuum detector. Specific surface area of the considered powders was measured by N_2 adsorption using Gemini V Micromeritics apparatus. Data were analyzed assuming Brunauer–Emmett–Teller (BET) isotherm.

3. Results and discussion

3.1. Crystal structure of $BaLnMn_2O_5$ and $BaLnMn_2O_6$ at room temperature

XRD measurements performed after synthesis (both, by soft chemistry and solid state methods) indicated formation of A-site ordered phase for all studied $BaLnMn_2O_{5+\delta}$ materials, as documented by (0 0 1) peak visible in the vicinity of 11.5° for oxidized and reduced compounds [30]. Exemplary XRD data with Rietveld refinement for $BaNdMn_2O_6$ II are shown in Fig. 1. Intensity of the mentioned (0 0 1) peak was significantly smaller for materials with larger Ln^{3+} cations, suggesting partial mixing between Ln and Ba. Despite good quality data, it was unfortunately not possible to reliably determine degree of such mixing, due to a similar atomic mass of Ln and Ba. For the completeness of the structural data, Table 1 presents results gathered for all considered materials (Ln: Pr, Nd, Sm, Gd, Dy, Er and Y), some of which were already presented in our previous works. As can be seen, with the decreasing ionic radius of Ln^{3+}, the relative increase of the normalized unit cell volume (i.e., divided to obtain cubic-like $1a_p \times 1a_p \times 1a_p$ unit cell) after the reduction process decreases, and the dependence between these two is linear ($R^2 = 0.996$). As the ionic radius of smaller Ln^{3+} is untypically small for 12-fold coordination, the normalized unit cell volume changes are weak in the case of such oxidized $BaLnMn_2O_6$. Structure of $BaPrMn_2O_6$ at room temperature (RT) was refined using aristotype $P4/mmm$ ($1a_p \times 1a_p \times 2a_p$) symmetry, consistent with previous report [22]. However, in the case of $BaNdMn_2O_6$ materials (from both synthesis methods), an evident split of (2 0 0) peak at ~46.5° was recorded at room temperature, indicating decrease of the crystal's symmetry. This distortion completely disappears already at 100 °C. It is known that in the vicinity of RT $BaNdMn_2O_6$ shows magnetic transitions, with the reported A-type antiferromagnetic ground state [31]. However, the magnetic phase diagrams elaborated in the literature differ significantly for this compound [21,22,24]. Therefore, it is not clear if the observed distortion can be connected to the presence of the

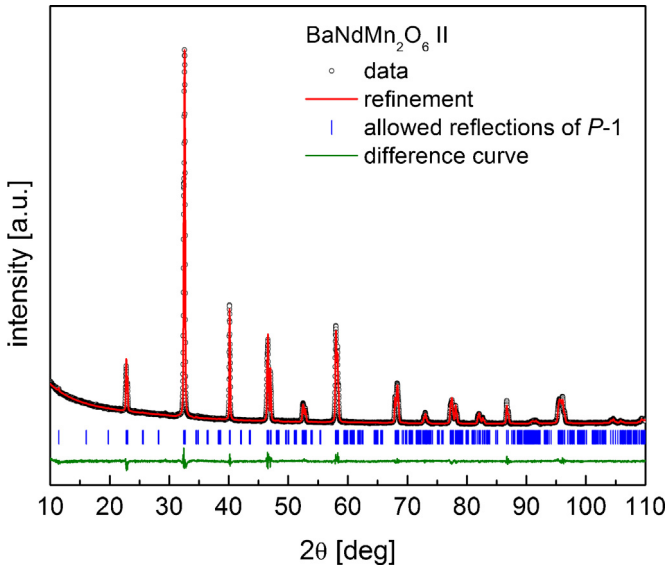

Fig. 1. Exemplary diffractogram with Rietveld analysis for $BaNdMn_2O_6$ II sample at room temperature refined assuming P-1 triclinic space group.

Table 1
Structural parameters of reduced and oxidized $BaLnMn_2O_{5+\delta}$ materials at room temperature.

Chemical composition	Space group	a (Å) b (Å) α (°) β (°)	c (Å) γ (°)	V (Å^3)	Relative increase of V after reduction[a]/ionic radius of Ln^{3+} in 8-fold coordination (Å)
$BaPrMn_2O_5$[b]	*P*4/*nmm*	5.6263(1)	7.7565(1)	245.53(1)	3.99%
$BaPrMn_2O_6$[b]	*P*4/*mmm*	3.9004(1)	7.7480(1)	117.87(1)	1.126
$BaNdMn_2O_5$	*P*4/*nmm*	5.6160(1)	7.7422(1)	244.18(1)	3.66%
$BaNdMn_2O_6$	*P*-1	5.5177(1) 5.5167(1) 90.00(3) 90.00(2)	7.7282(1) 90.10(1)	235.24(1)	1.109
$BaNdMn_2O_5$ II[c,d]	*P*4/*nmm*	5.6142(1)	7.7374(1)	243.88(1)	3.70%
$BaNdMn_2O_6$ II[c]	*P*-1	5.5139(1) 5.5137(1) 90.00(1) 90.00(1)	7.7247(1) 90.16(1)	234.85(1)	1.109
$BaSmMn_2O_5$[e]	*P*4/*nmm*	5.5963(1)	7.7105(1)	241.48(1)	3.01%
$BaSmMn_2O_6$[e]	*P*4/*nmm*	5.5430(1)	7.6227(1)	234.21(1)	1.079
$BaGdMn_2O_5$[f]	*P*4/*nmm*	5.5808(1)	7.6876(1)	239.43(1)	2.59%
$BaGdMn_2O_6$[f]	*P*4/*nmm*	5.5352(1)	7.6121(1)	233.23(1)	1.053
$BaDyMn_2O_5$	*P*4/*nmm*	5.5663(1)	7.6658(1)	237.18(1)	1.94%
$BaDyMn_2O_6$	*P*-1	5.5293(1) 5.5269(2) 90.00(1) 90.29(1)	7.6103(2) 89.95(1)	232.57(1)	1.027
$BaYMn_2O_5$[e]	*P*4/*nmm*	5.5496(1)	7.6548(1)	235.75(1)	1.54%
$BaYMn_2O_6$[e]	*P*-1	5.5253(1) 5.5198(1) 90.01(1) 90.30(1)	7.6105(1) 89.96(1)	232.11(1)	1.019
$BaYMn_2O_5$ II[c]	*P*4/*nmm*	5.5509(1)	7.6560(1)	235.90(1)	1.57%
$BaYMn_2O_6$ II[c]	*P*-1	5.5265(1) 5.5207(1) 90.00(1) 90.29(1)	7.6103(1) 89.94(1)	232.19(1)	1.019
$BaErMn_2O_5$[g]	*P*4/*nmm*	5.5424(1)	7.6422(1)	234.76(1)	1.31%
$BaErMn_2O_6$[g]	*P*-1	5.5206(1) 5.5147(1) 90.01(1) 90.29(1)	7.6100(1) 89.92(1)	231.68(1)	1.004

[a] Calculated using unit cell volumes normalized to *P*4/*nmm*.
[b] Data from Ref. [15].
[c] Synthesized by a solid state reaction method.
[d] Despite 220 min. reduction at 500 °C in 5 vol.% H_2 in Ar, the sample contained ~15 wt.% of $BaNdMn_2O_{5.5}$ phase (*Icma* symmetry [25]).
[e] Data from Ref. [28].
[f] Data from Ref. [29].
[g] Data from Ref. [14].

magnetic ordering. In order to unambiguously determine the actual symmetry and space group for this oxide, preferably neutron diffraction data are needed. For the oxidized (O_6) samples with smaller Ln^{3+} (Sm^{3+}, Gd^{3+}) cations, good refinement of the data was obtained assuming *P*4/*nmm* ($\sqrt{2}a_p \times \sqrt{2}a_p \times 2a_p$) superstructure, as reported in the literature [22]. In this structure, B-site (Mn) cations form rock salt-like charge order with (formal) Mn^{3+} and Mn^{4+} states at different crystallographic positions [17,32]. Moreover, in the case of even smaller Ln^{3+} (Dy^{3+}, Y^{3+} and Er^{3+}) the actual symmetry seems to be even lower, with suggested either monoclinic *P*121 or triclinic *P*-1 space groups [14,32–34]. The reported structural data for these compounds were refined using triclinic symmetry.

Structural data for all reduced $BaLnMn_2O_5$ compounds were refined using *P*4/*nmm* symmetry, in which B-site rock salt-like charge order of Mn^{2+} and Mn^{3+} cations is preserved. While there is no electronic phase diagram available for all $BaLnMn_2O_5$, supposedly all these materials possess significantly lower electrical conductivity than their oxidized counterparts (see for example data for $BaErMn_2O_{5+\delta}$ [14]), supporting choice of *P*4/*nmm* space group with distinctive sites for Mn^{2+} and Mn^{3+}.

3.2. Crystal structure changes during oxidation of $BaNdMn_2O_{5+\delta}$

It was reported that $BaYMn_2O_5$ oxidizes in air rapidly above 250 °C [1]. Similar results were also shown for $BaErMn_2O_5$ [14] and $BaY_{1-x}Pr_xMn_2O_5$ series [15]. However, such fast oxidation changes cannot be precisely monitored by *in situ* XRD studies. In the case of compounds synthesized by the solid state reaction at high temperatures (having larger grain size, as shown below) the oxidation process is slow enough to observe it during regular XRD scans. Such data for the oxidation of $BaNdMn_2O_5$ II sample are shown in Fig. 2a. It is worth noting that during the transformation, which for this particular material occurs at 200 °C, the recorded peak intensities are much lower, comparing to the ones observed before and after the oxidation. This may be understood, taking into

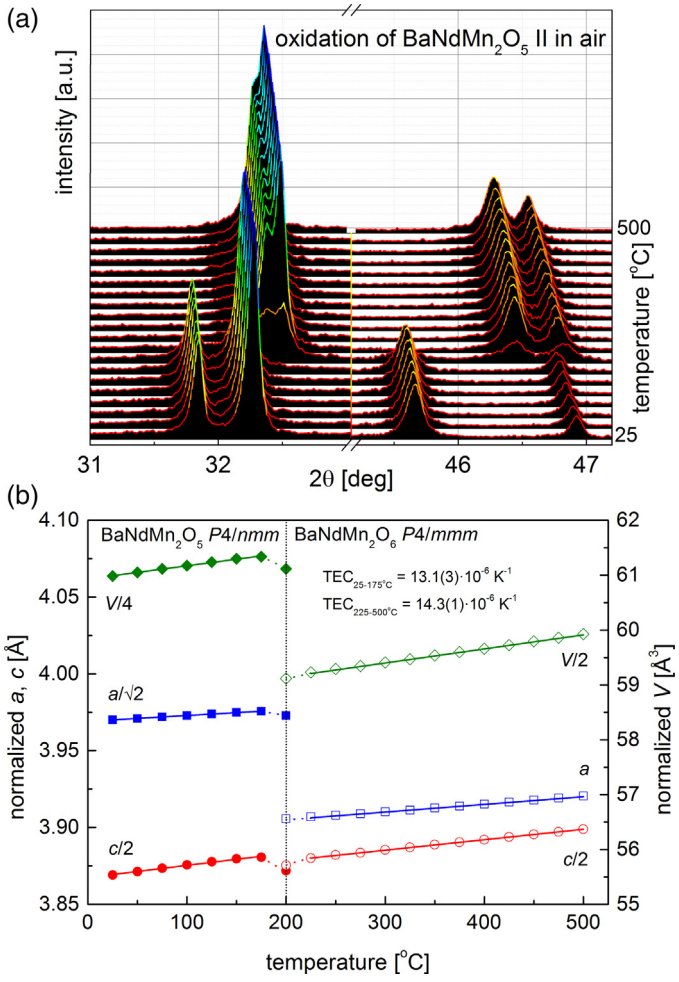

Fig. 2. (a) Structural evolution of reduced $BaNdMn_2O_5$ II sample during heating in air, data shown for selected angular range, (b) temperature dependence of normalized unit cell parameters and volume, together with calculated thermal expansion coefficients.

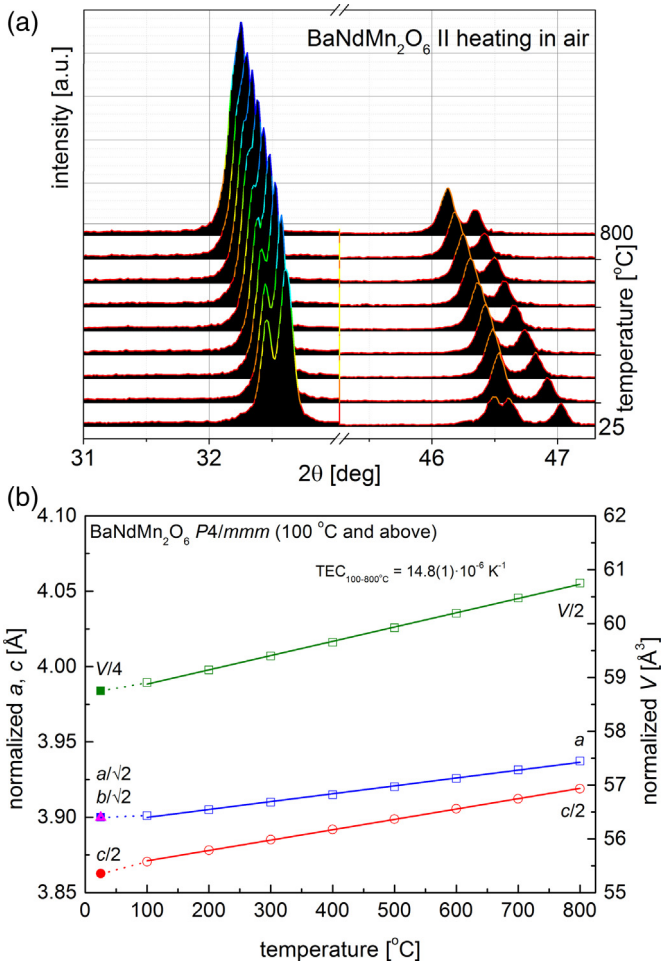

Fig. 3. (a) Structural evolution of oxidized $BaNdMn_2O_6$ II sample during heating in air, data shown for selected angular range, (b) temperature dependence of normalized unit cell parameters and volume, together with calculated thermal expansion coefficient.

account that during the oxidation the structural coherence length is significantly shortened, but after the process, the structure is in fact rebuilt. Using *in situ* XRD data it was possible to measure temperature dependence of the unit cell parameters and volume, as well as the actual change occurring during the oxidation. Such results, together with calculated thermal expansion coefficients are shown in Fig. 2b. For comparison, similar *in situ* data are also reported for the oxidized $BaNdMn_2O_6$ II compound, for which the only visible effects can be associated with the thermal expansion (Fig. 3a and b). One can also notice the mentioned disappearance of the structural distortion for the considered compound, comparing data recorded at 25 °C and 100 °C. Similar behavior upon oxidation can be expected for all other samples, however, materials obtained by the soft chemistry method oxidize too fast, to see the intermediate step on the XRD data.

Due to technical limitations it was not possible to use reducing atmosphere in Anton Paar HTK 1200N oven-chamber. Nevertheless, it is well known that the reduction process (even in a relatively strong reducing atmosphere of 5 vol.% H_2 in Ar at 500 °C [1,14,15]) takes much longer time (minutes), comparing to the oxidation (seconds). The origin of this behavior stems from the fact that the oxidation is rather strongly exothermic ($\Delta H \approx -220$ kJ mol^{-1} for $BaYMn_2O_5$ [16]), which causes local over-heating of the material, speeding up the diffusion of the oxygen in the bulk.

3.3. Oxygen storage properties of $BaLnMn_2O_{5+\delta}$

As shown by Motohashi et al. [1], $BaYMn_2O_6$ can be fully reduced to $BaYMn_2O_5$ in the atmosphere of 5 vol.% H_2 in Ar during heating up to 500 °C. A similar behavior is also characteristic for all considered $BaLnMn_2O_6$, as depicted in Fig. 4a. For these materials, the reduction is effective at temperatures of the order of 300–350 °C, with no obvious dependence on the ionic radius of Ln^{3+}. Among the studied compounds, only in the case of $BaYMn_2O_6$ sample, the reduction was not completed at 500 °C. However, the heating rate in this experiment was 5 times faster than the one reported in work [1]. For oxides with bigger Ln cation (i.e., Pr^{3+}, Nd^{3+} and Sm^{3+}), an inflection on the reduction curves can be noticed, indicating formation of the oxygen vacancy-ordered $BaLnMn_2O_{5.5}$. It is also worth noting that for $BaPrMn_2O_6$ material there is a slight decrease of the weight occurring at lower temperatures (30–250 °C). Oxidation behavior during heating in air is shown for all $BaLnMn_2O_5$ in Fig. 4b. In the case of this process, there is a clear dependence between radius of Ln^{3+} and the oxidation temperature, with oxides having bigger Ln^{3+} oxidizing at lower temperatures. Likely this results indicate similar dependence of the enthalpy of oxidation on the chemical composition of $BaLnMn_2O_5$, but needs further studies for clarification.

Systematically collected oxygen storage data for all $BaLnMn_2O_{5+\delta}$ are shown in Table 2. For all of the studied materials, the effective change of δ on reduction and oxidation, either during

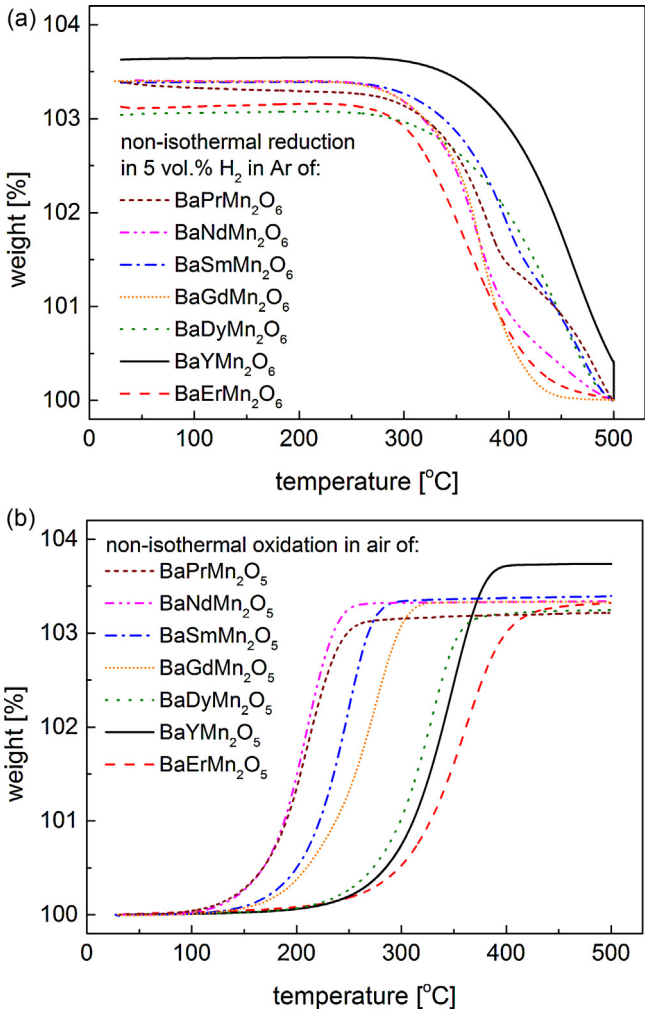

Fig. 4. Comparison of weight changes of (a) $BaLnMn_2O_5$ during heating in air up to 500 °C, (b) $BaLnMn_2O_6$ during heating in 5 vol.% H_2/Ar up to 500 °C. Data for $BaErMn_2O_6$ and $BaErMn_2O_5$ from Ref. [14].

non-isothermal heating or at 500 °C exceed 94% of the expected changes from $\delta = 0$ to $\delta = 1$. Obviously, Y-containing material has the highest theoretical (and practical) oxygen storage capacity (OSC), due to its lowest molar mass. Nevertheless, faster kinetics were measured during reduction of $BaGdMn_2O_6$.

Because reduction is the limiting process (oxidation is much faster), from the practical point of view of application, it is necessary to obtain materials with enhanced reduction kinetics. As can be expected, apart from chemical composition, also grain size

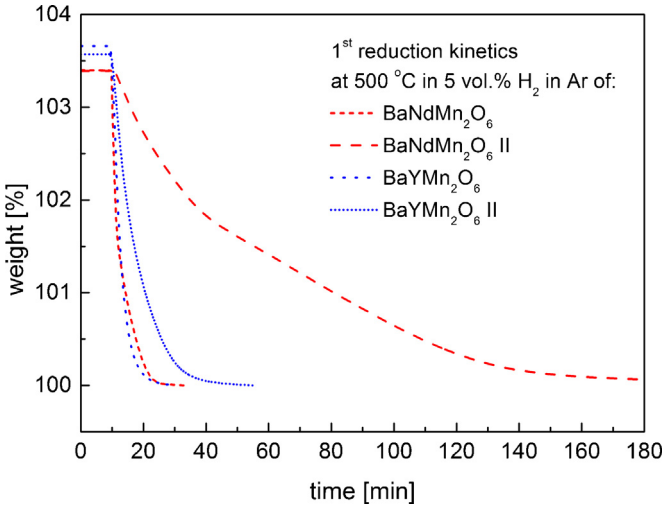

Fig. 5. Comparison of reduction kinetics for $BaNdMn_2O_6$ and $BaYMn_2O_6$ powders obtained by two different synthesis routes.

and morphology of the powder should have strong influence on the speed of reduction and oxidation [35]. Fig. 5 shows data concerning reduction of $BaNdMn_2O_6$ and $BaYMn_2O_6$ powders obtained by two different synthesis routes. In both of the cases, reduction of materials obtained by the solid state reaction was significantly slower. Clear difference in grain size and powder morphology for these samples can be noticed by analyzing SEM micrographs shown in Fig. 6a–d. Apart from about 10-fold smaller grains for $BaLnMn_2O_5$ obtained by the soft chemistry method, also, porous-like structure of agglomerates, which helps exchange of gasses and diffusion, is beneficial in terms of the speed of reduction. This in turn brings question, if the observed enhanced reduction speed for $BaGdMn_2O_6$ (Table 2) could be only related to the smaller grain size obtained for this particular sample. In order to clarify this, specific surface area was measured for the considered materials, and surprisingly, it was found to be 1.4 $m^2 g^{-1}$ for Gd-containing oxide, while for instance, for Y-containing one it was 2.4 $m^2 g^{-1}$, suggesting that also the chemical composition has strong effect on the reduction (and oxidation) behavior of $BaLnMn_2O_{5+\delta}$.

Interestingly, during consecutive isothermal cycles at 500 °C kinetics of the reduction are actually enhanced, as depicted in Fig. 7. For reduction of $BaGdMn_2O_6$ the oxygen release rate, as defined in work [35], reached 1.6 wt.% min^{-1} during the 5th reduction, matching the values obtained for the optimized $BaYMn_2O_6$ with larger specific surface area.

Table 2
Oxygen storage properties of the considered $BaLnMn_2O_{5+\delta}$ materials.

Chemical composition	Theoretical change of weight (wt.%)	Change of weight on reduction/oxidation (5th cycle at 500 °C) (wt.%)	Average change of weight on non-isothermal oxidation/reduction (%)	Temperature of oxidation (99% of total mass change) (°C)	Time of reduction (99% of total mass change, 5th reduction) (min)
$BaPrMn_2O_{5+\delta}$	3.42	3.34	3.30	360	11.0
$BaNdMn_2O_{5+\delta}$	3.39	3.33	3.37	260	14.5
$BaSmMn_2O_{5+\delta}$	3.35	3.32	3.40	300	13.8
$BaGdMn_2O_{5+\delta}$	3.30	3.32	3.36	315	4.5
$BaDyMn_2O_{5+\delta}$	3.27	3.16	3.14	415	11.2
$BaErMn_2O_{5+\delta}$	3.24	3.06	3.17	465[a]	10.0[a]
$BaYMn_2O_{5+\delta}$	3.85	3.71	3.68	395	10.9

[a] Data from Ref. [14].

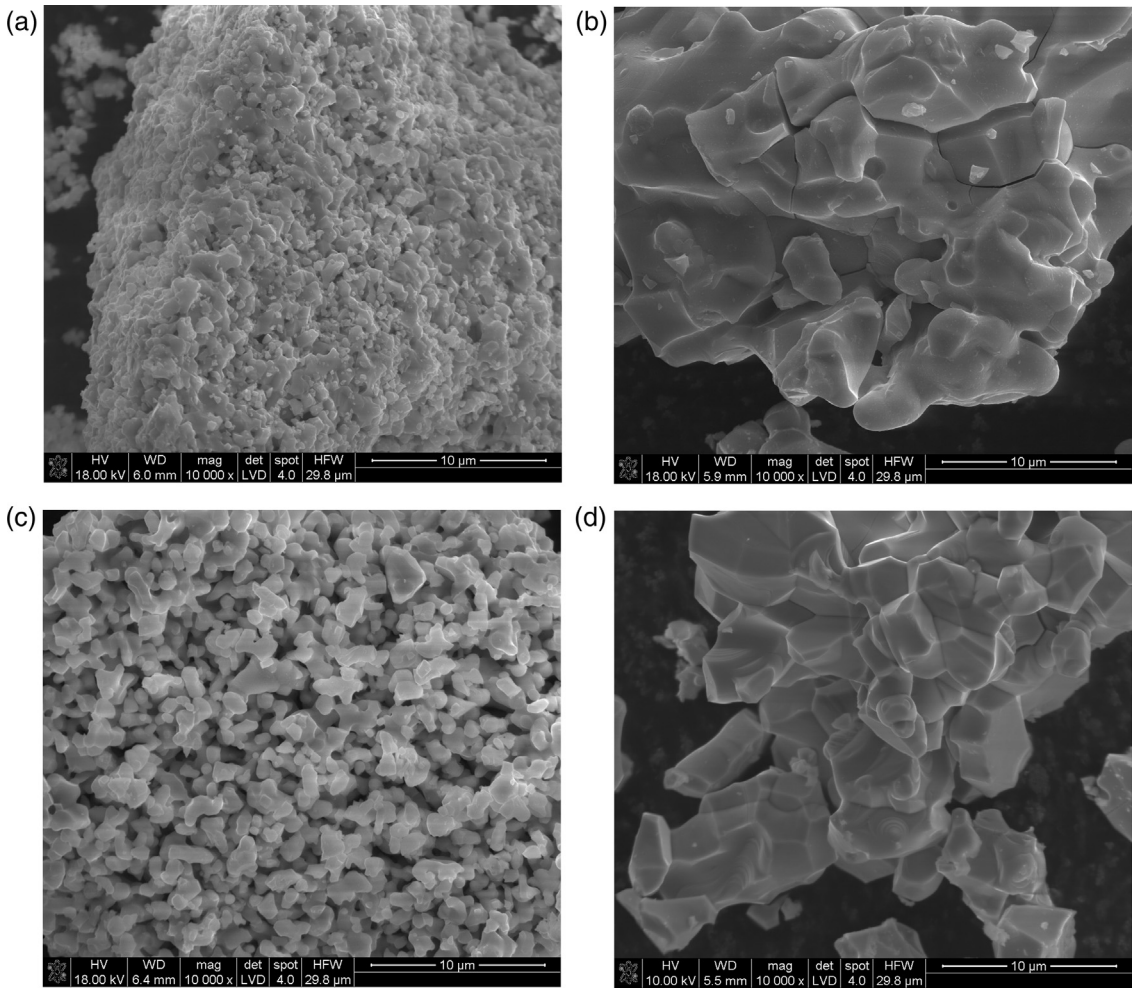

Fig. 6. SEM micrographs (10,000×) for (a) $BaNdMn_2O_5$, (b) $BaNdMn_2O_5$ II, (c) $BaYMn_2O_5$, and (d) $BaYMn_2O_5$ II.

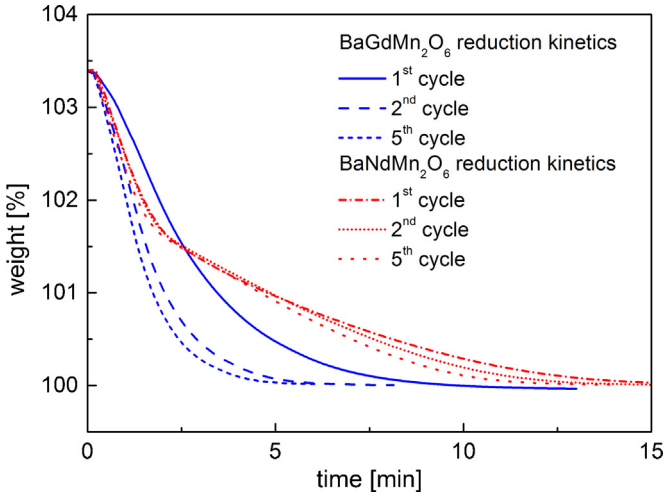

Fig. 7. Comparison of reduction kinetics for $BaGdMn_2O_6$ and $BaYMn_2O_6$ powders, as recorded during 1st, 2nd and 5th reduction. Data for 2nd reduction of $BaGdMn_2O_6$ from Ref. [28].

4. Conclusions

Crystal structure of reduced and oxidized A-site cation ordered $BaLnMn_2O_{5+\delta}$ (Ln: Pr, Nd, Sm, Gd, Dy, Er and Y) perovskite-type oxides was studied at room temperature showing different symmetry depending on the oxygen content and ionic radius of Ln^{3+}. *In situ* high temperature XRD measurements allowed to directly observe the ongoing structural changes during oxidation in air of $BaNdMn_2O_5$. The considered materials show practically complete and reversible change between reduced $BaLnMn_2O_5$ and oxidized $BaLnMn_2O_6$ (change of $\delta \approx 1$), which occurs at moderate temperatures (300–500 °C) during changes of the oxygen partial pressure (air, 5 vol.% H_2 in Ar). A systematic investigation performed for all $BaLnMn_2O_{5+\delta}$ allowed to conclude that both chemical composition and powder morphology are determining the kinetics of the reduction process.

Acknowledgements

The project was funded by the National Science Centre Poland (NCN) on the basis of the decision number DEC-2011/01/B/ST8/04046.

The authors (A.K., K.Ś., A.T.) acknowledge financial support from JSPS-PAN Joint Research Project “Development of IGFU System with Oxygen and Hydrogen Storage Units”.

References

[1] T. Motohashi, T. Ueda, Y. Masubuchi, M. Takiguchi, T. Setoyama, K. Oshima, S. Kikkawa, Chem. Mater. 22 (2010) 3192–3196.
[2] J. Kašpar, P. Fornasiero, J. Solid State Chem. 171 (2003) 19–29.
[3] M. Machida, K. Kawamura, K. Ito, K. Ikeue, Chem. Mater. 17 (2005) 1487–1492.
[4] M. Karppinen, H. Yamauchi, S. Otani, T. Fujita, T. Motohashi, Y.-H. Huang, M. Valkeapää, H. Fjellvåg, Chem. Mater. 18 (2) (2006) 490–494.

[5] T. Motohashi, S. Kadota, H. Fjellvåg, M. Karppinen, H. Yamauchi, Mater. Sci. Eng. B 148 (2008) 196–198.
[6] P. Singh, M.S. Hedge, J. Gopalakrishnan, Chem. Mater. 20 (23) (2008) 7268–7273.
[7] M. Sugiura, Catal. Surv. Asia 7 (2003) 77–87.
[8] Z. Yang, Y.S. Lin, Y. Zeng, Ind. Eng. Chem. Res. 41 (2002) 2775–2784.
[9] D.J.L. Brett, A. Atkinson, N.P. Brandon, S.J. Skinner, Chem. Soc. Rev. 37 (2008) 1568–1578.
[10] A. Trovarelli, Catalysis by Ceria and Related Materials, Imperial College Press, London, 2002.
[11] M. Machida, K. Kawamura, T. Kawano, D. Zhang, K. Ikeue, J. Mater. Chem. 16 (2006) 3084–3090.
[12] O. Adamopoulos, E. Björkman, Y. Zhang, M. Muhammed, T. Bog, L. Mussmann, E. Lox, J. Eur. Ceram. Soc. 29 (2009) 677–689.
[13] Z.M. Shi, Y. Liu, W.Y. Yang, M.K. Liang, F. Pan, S.R. Gu, J. Eur. Ceram. Soc. 22 (2002) 1251–1256.
[14] K. Świerczek, A. Klimkowicz, Z. Zheng, D. Dabrowski, J. Solid State Chem. 203 (2013) 68–73.
[15] A. Klimkowicz, K. Świerczek, K. Zheng, M. Baranowska, A. Takasaki, B. Dabrowski, Solid State Ionics 262 (2014) 659–663.
[16] M. Gilleßen, M. Lumeij, J. George, R. Stoffel, T. Motohashi, S. Kikkawa, R. Dronskowski, Chem. Mater. 24 (2012) 1910–1916.
[17] G. King, P.M. Woodward, J. Mater. Chem. 20 (2010) 5785–5796.
[18] F. Millange, E. Suard, V. Caignaert, B. Raveau, Mater. Res. Bull. 34 (1) (1999) 1–9.
[19] I.O. Troyanchuk, S.V. Trukhanov, G. Szymczak, Crystallogr. Rep. 47 (4) (2002) 658–665.
[20] T. Nakajima, H. Kageyama, Y. Ueda, Phys. B 329–333 (2003) 844–845.
[21] T. Nakajima, H. Kageyama, H. Yoshizawa, Y. Ueda, J. Phys. Soc. Jpn. 71 (12) (2002) 2843–2846.
[22] Y. Ueda, T. Nakajima, J. Phys. Condens. Matter 16 (2004) 573–583.
[23] R.H. Mitchell, Perovskites Modern and Ancient, Almaz Press Inc., Canada, 2002.
[24] D. Akahoshi, Y. Okimoto, M. Kubota, R. Kumai, T. Arima, Y. Tomioka, Y. Tokura, Phys. Rev. B 70 (2004) 064418-1-7.
[25] C. Perca, L. Pinsard-Gaudart, A. Daoud-Aladine, M.T. Fernández-Díaz, J. Rodríguez-Carvajal, Chem. Mater. 17 (2005) 1835–1843.
[26] A.C. Larson, R.B. Von Dreele, Los Alamos Natl. Lab. Rep. – LAUR 86-748, 2004
[27] B.H. Toby, J. Appl. Crystallogr. 34 (2001) 210–213.
[28] A. Klimkowicz, K. Zheng, G. Fiołka, K. Świerczek, Ceram. Mater. 65 (1) (2013) 92–96.
[29] A. Klimkowicz, K. Zheng, G. Fiołka, K. Świerczek, Chemik 67 (12) (2013) 1202–1205.
[30] S.V. Trukhanov, I.O. Troyanchuk, M. Hervieu, H. Szymczak, K. Bärner, Phys. Rev. B 66 (2002) 184424-1-10.
[31] Y. Miyauchi, A. Mitsuru, D. Akahoshi, H. Kuwahara, J. Phys. Soc. Jpn. 80 (2011) 074708-01-03.
[32] A.J. Wiliams, J.P. Attfield, Phys. Rev. B 72 (2005) 024436-1-5.
[33] T. Nakajima, H. Kageyama, Y. Ueda, J. Phys. Chem. Solids 63 (2002) 913–916.
[34] M. Karppinen, H. Okamoto, H. Fjellvåg, T. Motohashi, H. Yamauchi, J. Solid State Chem. 177 (2004) 2122–2128.
[35] T. Motohashi, T. Ueda, Y. Masubuchi, S. Kikkawa, J. Ceram. Soc. Jpn. 119 (11) (2011) 894–897.